# Multiparametric Non-Negative Matrix Factorization for Longitudinal Variations Detection in White-Matter Fiber Bundles

Claudio Stamile, Gabriel Kocevar, François Cotton, Frederik Maes, Dominique Sappey-Marinier, and Sabine Van Huffel, *Fellow, IEEE*

***Abstract*—Processing of longitudinal diffusion tensor imaging (DTI) data is a crucial challenge to better understand pathological mechanisms of complex brain diseases such as multiple sclerosis (MS) where white-matter (WM) fiber bundles are variably altered by inflammatory events. In this study, we propose a new fully automated method to detect longitudinal changes in diffusivity metrics along WM fiber bundles. The proposed method is divided in three main parts: 1) preprocessing of longitudinal diffusion acquisitions, 2) WM fiber-bundle extraction, and 3) application of nonnegative matrix factorization and density-based local outliers algorithms to detect and delineate longitudinal variations appearing in the cross section of the WM fiber bundle. In order to validate our method, we introduce a new model to simulate real longitudinal changes based on a generalized Gaussian probability density function. Moreover, we applied our method on longitudinal data. High level of performances were obtained for the detection of small longitudinal changes along the WM fiber bundles in MS patients.**

***Index Terms*—Longitudinal analysis, multiple sclerosis (MS), nonnegative matrix factorization, tractography, white matter (WM).**

Manuscript received March 14, 2016; revised July 7, 2016; accepted August 1, 2016. Date of publication August 3, 2016; date of current version September 1, 2017. This work was supported in part by the Flemish Government FWO project G.0869.12N (Tumor imaging); in part by the Belgian Federal Science Policy Office: IUAP P7/19/ (DYSCO, "Dynamical systems, control and optimization", 2012–2017); in part by the Henri Benedictus Fellowship of the Belgian American Educational Foundation; in part by the French National Research Agency (ANR) within the national program "Investissements d'Avenir" through the OFSEP project (ANR-10-COHO-002); in part by the European Research Council under the European Union's Seventh Framework Programme (FP7/2007-2013) / ERC Advanced Grant: BIOTENSORS (339804); and in part by EU MC ITN TRANSACT 2012 (316679).

C. Stamile is with CREATIS, CNRS UMR5220, INSERM U1044, INSA-Lyon, Université de Lyon 1, 69100, Villeurbanne, France, and also with Department of Electrical Engineering (ESAT), STADIUS Center for Dynamical Systems, Signal Processing and Data Analytics, Katholieke Universiteit Leuven, 3000, Leuven, Belgium (e-mail: stamile@creatis.insa-lyon.fr).

G. Kocevar is with CREATIS, CNRS UMR5220, INSERM U1044, INSA-Lyon, Université de Lyon 1, 69100, Villeurbanne, France (e-mail: kocevar@creatis.insa-lyon.fr).

F. Cotton is with CREATIS, CNRS UMR5220, INSERM U1044, INSA-Lyon, Université de Lyon 1, 69100, Villeurbanne, France, and also with Service de Radiologie, Centre Hospitalier Lyon-Sud, Hospices Civils de Lyon, 69310, Pierre-Bénite, France (e-mail: francois.cotton@chu-lyon.fr).

F. Maes is with the PSI Processing Speech and Images, Department of Electrical Engineering (ESAT), Katholieke Universiteit Leuven, 3000, Leuven, Belgium (e-mail: Frederik.Maes@esat.kuleuven.be).

D. Sappey-Marinier is with CREATIS, CNRS UMR5220, INSERM U1044, INSA-Lyon, Université de Lyon 1, 69100, Villeurbanne, France, and also with CERMEP—Imagerie du Vivant, Université de Lyon, 69007, Lyon, France (e-mail: dominique.sappey-marinier@univ-lyon1.fr).

S. Van Huffel is with the Department of Electrical Engineering (ESAT), STADIUS Center for Dynamical Systems, Signal Processing and Data Analytics, Katholieke Universiteit Leuven, 3000, Leuven, Belgium, and also with Medical Information Technologies Department, iMinds, 3000, Leuven, Belgium. (e-mail: sabine.vanhuffel@esat.kuleuven.be).

Digital Object Identifier 10.1109/JBHI.2016.2597963

## I. Introduction

ANALYSIS and processing of longitudinal magnetic resonance imaging (MRI) data is a crucial problem in image analysis. Since pathological mechanisms remained unknown in certain brain diseases, the investigation of their temporal progression using noninvasive neuroimaging techniques is essential to better understand and predict the disease evolution and manage the therapeutic treatment [1], [2]. As the etiology of multiple sclerosis (MS) as well as the pathological mechanisms including inflammatory and neurodegenerative processes, are not well understood, longitudinal studies using advanced MRI techniques such as diffusion tensor imaging (DTI) providing sensitive markers of the underlying tissue microstructure, such as fractional anisotropy (FA) and radial diffusivity ($\lambda_r$), constitute the best potential for the characterization of brain tissue alterations. For example, the analysis of gray matter (GM) structures [3] showed the capability to evaluate the dynamics disease progression; in white matter (WM) [4], a relationship between damaging and repairing mechanisms that occur in the lesions formation is revealed. By merging the spatial information of fiber tracking [5] with the diffusion metrics derived from the diffusion tensor, it is possible to characterize the presence of "pathological" events that may occur along afferent WM fiber pathways leading to antero- or retrograde degeneration. Thus, for a better understanding of the spatial and temporal progression of MS pathological processes, an accurate and sensitive characterization of WM fibers along their pathways is needed. As shown in our previous work [6], a global approach to analyze disease evolution was not sensitive enough to detect small and short-term (daily/weekly) longitudinal variations occurring typically in relapsing remitting (RR) MS patients. A local scale approach is thus necessary to detect the presence of small "pathological" changes that could only affect a small subset

2168-2194 © 2016 IEEE. Personal use is permitted, but republication/redistribution requires IEEE permission.
See http://www.ieee.org/publications_standards/publications/rights/index.html for more information.

of the WM fiber bundle. A first model was proposed in [7]. Due to its simplicity, important assumptions about classical longitudinal biases like noise and registration errors [8] are not taken into account. In order to overcome this limitation in [9], we proposed a genetic algorithm to detect longitudinal variations on the FA histogram occurring along WM fiber bundles in MS patients. In this model, assumptions about noise and registration errors are taken into account in order to detect pathological longitudinal variations. Unfortunately the model is limited by its computational complexity. Since it is based on a genetic algorithm the analysis of a specific region could take a large amount of time. Moreover another limitation of the models [7], [9] is given by their incapability to manage multimodal/parametric data and multiple time points.

In order to overcome all these limitations, in this study, we present a new fully automated method based on nonnegative matrix factorization (NMF). The method allows using multiparametric DTI-derived metrics to detect small longitudinal variations occurring along WM fiber bundles in MS patients. Since NMF is a blind source separation (BSS) technique, we do not need to provide a model to describe the temporal evolution of the pathology in the brain tissues.

This paper is structured as follows. In Section II, we provide a detailed description of our approach. In Section III, we present our experimental campaign. In Section IV, we show our results. In Section V, we discuss the performances, benefits, and limitations of our method. Finally, in Section VI, we draw our conclusions.

## II. Description of the Proposed Approach

The proposed method is divided in three main parts: 1) preprocessing of longitudinal diffusion acquisitions, 2) WM fiber bundle extraction, and 3) application of NMF and density-based local outliers (LOF) algorithms to detect and delineate longitudinal variations appearing in the cross section of the WM fiber bundle.

### A. Data Preprocessing

As first step, each of the $t$ time points ($T_1 \dots T_t$) of DTI longitudinal acquisitions, are processed. Eddy current correction [10] was first applied on the diffusion volumes using the b0 volume ($b = 0$ s.mm$^{-2}$) as reference. The corrected volumes were then used in order to compute the tensor model using the FDT module of FSL [10]. Longitudinal data coregistration is performed using the method described in [11] based on DTI ToolKit (DTI-TK) including the following procedures: 1) generation of a patient-specific template obtained from longitudinal diffusion tensor images, 2) coregistration of the resulting template to the Illinois Institute of Technology (IIT) atlas [12], and 3) coregistration of each time-point data into the IIT atlas space by applying the previously obtained transformations to the initial longitudinal data. The resulting tensor image is then used to compute six diffusion metric maps: FA, mean diffusivity (MD), and radial diffusivity ($\lambda_r$) and the three eigenvalues of the diffusion tensor ($\lambda_1$, $\lambda_2$, $\lambda_3$). Moreover, two diffusion anisotropy measurements were computed: Compositional Kullback–Leibler anisotropy (KLA) and angular anisotropy (AA) [13].

### B. Fiber-Bundle Extraction

Probabilistic streamline tractography was performed using MRTrix [14] based on the fiber-orientation density information of the IIT Atlas. Twenty fiber bundles were extracted using a semiautomatic algorithm [15] coupled with the prior knowledge extracted from the 20 regions of interest of the johns hopkins university (JHU) fiber-bundle atlas [16]. In order to analyze fiber bundles an additional step is needed. Indeed the output of the tractography could not be directly used for the analysis of the fiber bundle since the number of points used to reconstruct the fibers varies. Moreover, start and end point of each fiber are not consistent within the same fiber bundle. Fibers could start randomly from the two extremities of the bundle. In order to overcome those problems part of the pipeline described in [6] was applied to process the fiber bundle. As first step, we define common start/end points of each fiber within the bundle. A classical K-means algorithm [17] is performed to generate two different clusters, $R_1$ for the starting points and $R_2$ for the ending points. Fiber points are then reordered from $R_1$ to $R_2$ and fibers that did not link the two clusters (broken fibers) are automatically removed. As final postprocessing step each fiber is resampled with the same number $c = 100$ of points (also called nodes).

After the postprocessing, we can formalize the extracted fiber bundle as set $F = \{f_1, f_2, \dots, f_n\}$ composed of $n$ fibers $f_i = \{\boldsymbol{p_1}, \dots, \boldsymbol{p_c}\}$ where $\boldsymbol{p_q} = (x_q, y_q, z_q) | 1 \leq q \leq c$. The coordinate $\boldsymbol{p_q}$ is used to extract the voxel's value of one of the six diffusion maps ($FA(\boldsymbol{p_q})$ in case of FA) in the corresponding location of $f_i$. By fixing the index $q$ in each fiber $f \in F$ it is possible to analyze the global diffusion values in a particular cross section of $F$. More in detail we can collect all the FA values belonging to a given cross section of $F$ defining the following set: $R_q = \{FA(\boldsymbol{p_q}) | \boldsymbol{p_q} \in f \forall f \in F\}$ where $q$ is the fixed index representing the cross section to analyze.

### C. NMF-Based Algorithm for Longitudinal Change Detection

The NMF-based model to detect longitudinal changes is composed of two main steps: 1) recursive application of the NMF algorithm to the data and 2) detection of "time-point outliers" in the source matrix $W$.

*1) Recursive Application of NMF:* NMF is a BSS technique [18], in which a data matrix $V$ is approximately factorized into the product of a source matrix $W$ and an abundance matrix $H$ as

$$V \approx W \times H.$$

$V \in \mathbb{R}^{n \times r}$ is a set of nonnegative data, with $r$ data points along its columns and $n$ features per data point on its rows. The columns of $W \in \mathbb{R}^{n \times k}$ represent the $k$ sources. $H \in \mathbb{R}^{k \times r}$ contains per column the abundance of each of the $k$ sources for one particular data point. In this way, NMF describes each point in a dataset by a linear combination of a predefined number of sources.

In particular, NMF-based methods have been applied successfully in MRI-based tumor segmentation [19], [20], [21]. NMF aims to extract physically meaningful sources, corresponding to tissue-specific patterns. It is an unsupervised technique, i.e., it

**Algorithm 1:** Algorithm for recursive NMF.

rNMF $(N, cl, l, \omega)$;
**Input**: $N$ root node containing the matrix to factorize, $cl$ current level of the tree (initialized to zero), $l$ total depth of the tree, $\omega$ threshold parameter
**Output**: $T$ tree containing the recursive factorization
**if** $l == cl$ **then**
  return $T$;
**else**
  $[H, W] \leftarrow NMF(N_V)$;
  $V_1 = \{v \in V[i,j] \mid \forall\ d_j \in D\ H[1,d_j] \geq \omega\}$;
  $V_2 = \{v \in V[i,j] \mid \forall\ d_j \in D\ H[2,d_j] \geq \omega\}$;
  $N_1 \leftarrow (V_1, H[1,:], W[:,1])$;
  $N_2 \leftarrow (V_2, H[2,:], W[:,2])$;
  $T \leftarrow$ addLeftChild$(N, N_1)$;
  $T \leftarrow$ addRightChild$(N, N_2)$;
  return rNMF$(N_1, cl+1, l, \omega)$;
  return rNMF$(N_2, cl+1, l, \omega)$;
**end**

can be applied on a patient-by-patient basis without the need for any training dataset. NMF assesses the relative contribution of each tissue type within each voxel, assuming the dataset can be modeled as a linear combination of the constituent tissue types. The mathematical formulation of the basic NMF problem to perform the factorization is given as follows:

$$\begin{aligned} \underset{\boldsymbol{W},\boldsymbol{H}}{\text{minimize}} \quad & f(\boldsymbol{W},\boldsymbol{H}) = \frac{1}{2}\|V - W \times H\|_F^2 \\ \text{subject to} \quad & \forall i,j : W_{i,j}, H_{i,j} \geq 0. \end{aligned}$$

Let $\boldsymbol{v} \in \mathbb{R}^3$ be a voxel of a given image $I$. We define as $I(\boldsymbol{v})$ the intensity value of the image $I$ in the voxel $\boldsymbol{v}$. Let $m$ be the number of DTI maps used in the analysis, in our longitudinal framework, we define as $I_{i,M_j}$ the image of DTI-derived map $M_j 1 \leq j \leq m$ acquired at time point $1 \leq i \leq t$.

Since we apply the algorithm in each cross section separately, we define with $D$ ($|D| = s$) the set of voxels $d_j \in \mathbb{R}^3, j = 1, \ldots, s$ contained in the specific cross-section of the fiber bundle to analyze.

Our NMF method is based on a sequential application of NMF as described in algorithm 1.

In the first level, the data matrix $V \in \mathbb{R}^{t*m \times s}$ containing the longitudinal signal information is factorized in $k = 2$ sources using NMF. The matrix is defined as

$$V = \begin{array}{c} \\ I_{1,M_1} \\ \vdots \\ I_{1,M_m} \\ \vdots \\ I_{tM_1} \\ \vdots \\ I_{t,M_m} \end{array} \begin{array}{c} \begin{array}{cccc} d_1 & d_2 & \ldots & d_s \end{array} \\ \begin{pmatrix} v^1_{1,1} & v^1_{1,2} & \ldots & v^1_{1,s} \\ \vdots & \vdots & \ddots & \vdots \\ \ldots & v^1_{m,2} & \ldots & v^1_{m,s} \\ \vdots & \vdots & \ddots & \vdots \\ \ldots & \ldots & \ldots & \ldots \\ \vdots & \vdots & \ddots & \vdots \\ \ldots & \ldots & \ldots & \ldots \end{pmatrix} \end{array}.$$

$V$ contains the voxels intensity for each of the $m$ DTI metrics in each of the $t$ time points ($I_{i,M_j} 1 \leq i \leq t, 1 \leq j \leq m$) for all the voxels $d_j \in D$ extracted in a given cross section $q$.

The application of the first level of our hierarchical NMF model to $V$ allows to obtain a source matrix $W$ and an abundance matrix $H$. In this paper, $W_1$ and $W_2$ denote, respectively, the two source vectors obtained from the first and the second column of $W$. Similarly, $H_1$ and $H_2$ denote, respectively, the two abundance vectors obtained from the first and the second row of $H$.

Let $h_{i,j} \in H$ be the $j$-th element of the $i$-th abundance vector, the elements in the $k$ (in our case, $k = 2$) vectors are normalized according to the following equation:

$$h_{i,j} = \frac{h_{i,j}}{\sum_{r=1}^{k} h_{r,j}} \quad \forall 1 \leq j \leq s\ ,\ 1 \leq i \leq k. \tag{1}$$

The normalized vectors are used to split the voxel set $D$ in two sets $(D_1, D_2)$ according to the following rule: $D_1 = \{d_j \in D | H[1,d_j] \geq \omega\}$ and $D_2 = \{d_j \in D | H[2,d_j] \geq \omega\}$ where $\omega \in \mathbb{R}$ is a given threshold. Similarly to $V$, we can generate two new data matrices $V_1$ and $V_2$ using, respectively, the voxels contained in $D_1$ and $D_2$. The NMF factorization could then be applied recursively to $V_1$ and $V_2$ in order to create a second level of matrices generated by the factorization. In general, the algorithm 1 could be applied to generate $l \in \mathbb{N}$ levels. The recursive application of NMF to each level could be formalized using a tree (see Fig. 2). Each level of the tree contains the abundance vector ($H_{i\ldots}$), the source vector ($W_{i\ldots}$), and the data matrix ($V_{i\ldots}$) obtained from the application of NMF of the previous level data.

*2) Detection of "Time-Point Outliers" in the Source Matrix:* In order to check, and eventually, isolate voxels affected by longitudinal changes, abundance and source vectors obtained at the lowest level of the hierarchy (the leaves of the tree) are used. If the analysis of the abundance vectors gives information about the single voxel, the analysis of the source vectors gives information about the contribution of each diffusion feature in each time point. In the rest of this section, we assume that $V_*$, $H_{*1}, H_{*2}$ and $W_{*1}, W_{*2}$ are, respectively, the data matrix, abundance and source vectors obtained in a generic leaf of the tree. In order to detect if, during the longitudinal follow-up, longitudinal variations are present we look for the presence of anomalies in the source vectors. More in detail, we say that a longitudinal variation appears during the follow-up if longitudinal variations are present in all the diffusion metrics belonging to certain time points of $W$ (see Fig. 3). We define these "changed time points" as *outliers*. In order to detect these points, the LOF algorithm [22] is used. This clustering algorithm allows to detect outliers by computing the LOF value for each element in the cluster. The LOF value of each object represents the degree of the object to be an outlier compared to the other elements in the cluster. This value strongly depends on a single parameter *MinPts*, which represents the number of nearest neighbors used in defining the local neighborhood of the object [22]. The main problem related to the LOF is the difficulty to interpret resulting LOF scores since there are no clear rules that define when a point is an outlier. In order to properly detect the outliers, this value should be carefully selected for the specific dataset. For a given source vector $W_g$, the input of the LOF algorithm is a matrix $F \in \mathbb{R}^{t \times m}$ where $f_{i,j} \in F$ contains the contribution of the $j$-th diffusion parameter at the $i$-th time point. The LOF algorithm

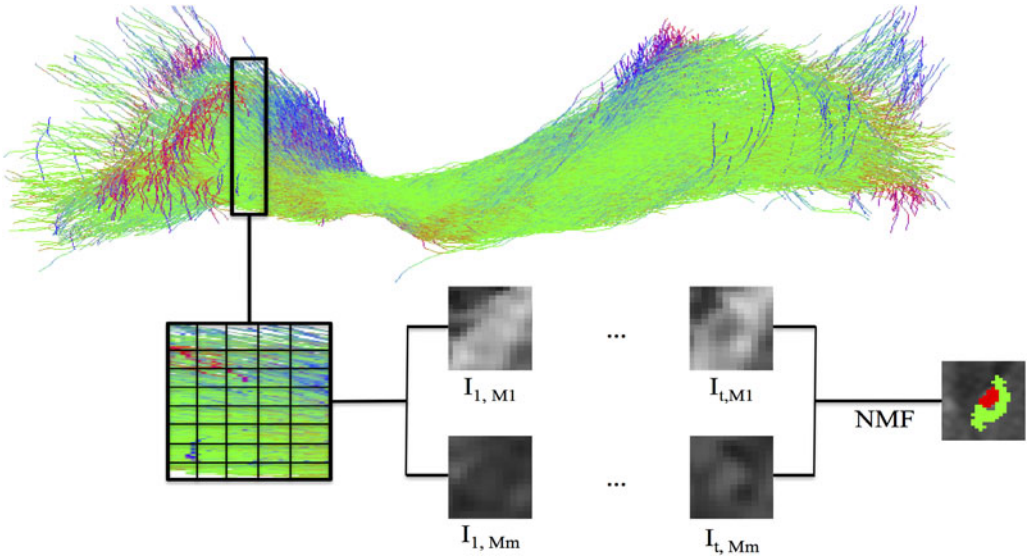



Fig. 1. Extraction of all $M_i$ signals in a cross section of the fiber bundle from time point 1 to $t$ and application of our NMF method to detect longitudinal variations.

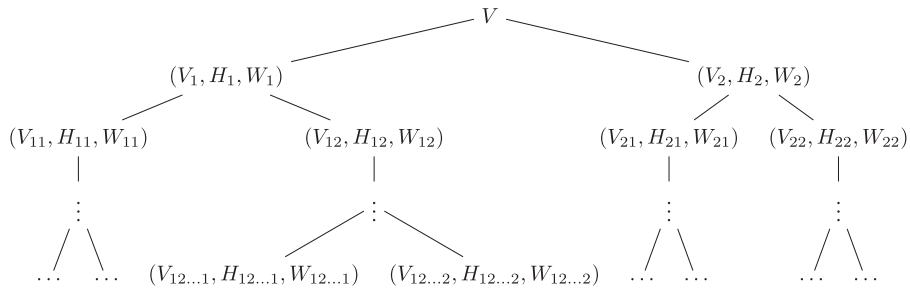



Fig. 2. Tree generated by the recursive application of NMF.

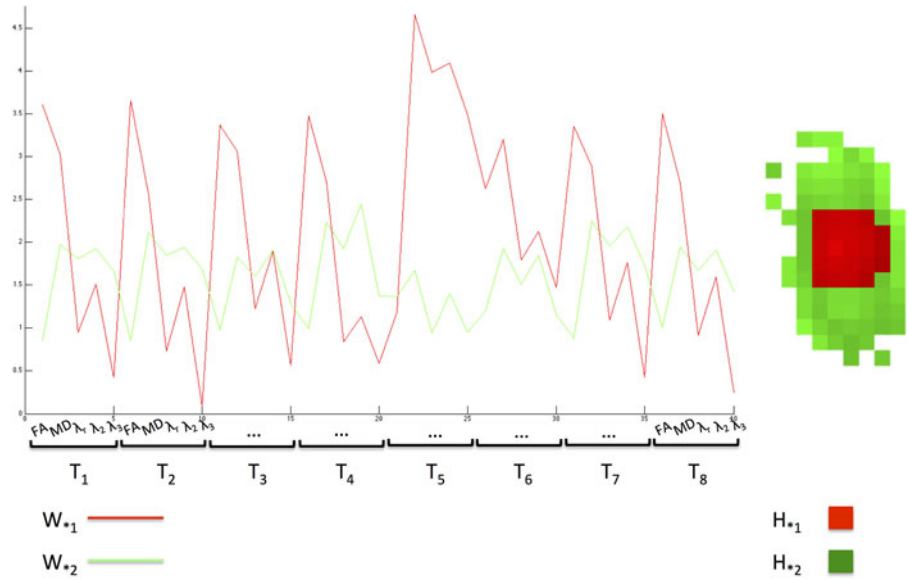



Fig. 3. On the left, the NMF source vectors ($W_{*1}$, $W_{*2}$) of one leaf of the tree. For each of the eight time points with $m = 5$, diffusion metrics (FA, MD, $\lambda_r$, $\lambda_2$, $\lambda_3$) are used for a total of 40 features. The outliers' peak visible at time point 5 ($T_5$) shows that the longitudinal alteration appears only at $T_5$. On the right, the voxels segmented using the information contained in the abundance vectors.

is then applied independently to $W_{*1}$ and $W_{*2}$. If outliers are detected in one of the two source vectors ($W_{*1}, W_{*2}$), the voxels belonging to the corresponding abundance matrix ($H_{*1}$, $H_{*2}$) having value $\geq \omega$ are marked as "evolving voxels" (see Fig. 3). These voxels delineate the region in the image affected by the longitudinal variation.

### D. Subjects

Five relapsing-remitting (RR) MS patients (four women and one man, mean ($\pm$SD) age: 36.8 $\pm$ 9.5 years; median disease duration: 4.24 years; max 16.5 years) (median expanded disability status scale = 2.5, range = [0; 4]) and one healthy control (HC) subject (age: 24 years) were included in this study. Inclusion criteria specified that studied patients were diagnosed as RR MS if they present at least one new Gadolinium-enhancing lesion during the six months preceding study enrollment. All patients had stopped their treatment for at least one year and have not started any during the study period. In order to limit the nephrogenic damage risks associated to Gadolinium injection, creatinine clearance was checked every 2 weeks after inclusion. A clearance higher than 60 ml/min was an exclusion criterion. This study was approved by the local ethics committee (CPP Lyon Sud-Est IV) and the French national agency for medicine and health products safety (ANSM). Written informed consent was obtained from all patients and the control subject prior to study initiation.

### E. MRI Protocol

All subjects underwent a weekly examination for a period of two months (eight time points from $T_1$ to $T_8$). The MRI protocol included a DTI and an FLAIR acquisition, that were performed on a 3T Philips Achieva system (Philips Healthcare, Best, The Netherlands) with a 16-channels head coil. The DTI image set consisted of the acquisition of 60 contiguous 2-mm-thick slices parallel to the bicommissural plane (AC-PC), and were acquired using a 2-D echo-planar imaging sequence (TE/TR = 60/8 210 ms, FOV = 224 $\times$ 224 $\times$ 120 mm) with 32 gradient directions (b =1000 s $\cdot$ mm$^{-2}$). The nominal voxel size at acquisition (2 $\times$ 2 $\times$ 2 mm) was interpolated to 0.875 $\times$ 0.875 $\times$ 2 mm after reconstruction. The FLAIR Vista 3-D sequence (TE/TR/TI = 356/8000/2400 ms, FOV=180 $\times$ 250 $\times$ 250 mm) consisted of the acquisition of 576 slices of 0.43-mm thickness.

### F. Longitudinal Variations Simulator (LVS)

As in [7], in order to generate real differences between scans such as noise induced by acquisition and changes in subject positioning, our algorithm was tested on simulated longitudinal changes generated along different fiber bundles in the control subject described in Section II-D.

In this section, we describe a new model to simulate pathological longitudinal changes on multiparametric diffusion data. The idea behind our model is the simulation of the MS longitudinal changes using two properties: shape size and diffusion value changes. We assume that the variation takes a spherical shape of radius $r$ that could change on time. Moreover, we assume that diffusion values of voxels belonging to this region could change during the longitudinal evolution of a factor $\rho$, called reduction coefficient. This coefficient $\rho$ is used to change the voxel's diffusion values inside the spherical region in a given time point according to the following equations:

$$\lambda_2^* = \lambda_2 + \rho * (\lambda_1 - \lambda_2) \qquad \lambda_3^* = \lambda_3 + \rho * (\lambda_1 - \lambda_3)$$

with $0 \leq \rho \leq 1$. FA, MD, and other tensor metrics are then recomputed in the given time point using $\lambda_1$ and the new $\lambda_2^*, \lambda_3^*$ values.

The proposed LVS model could be summarized using the parametric function $S$ defined as

$$S : \begin{cases} r(t) = \mathcal{G}(t, \mu_r, \alpha_r, \beta_r) \\ \rho(t) = \mathcal{G}(t, \mu_\rho, \alpha_\rho, \beta_\rho) \end{cases}$$

the function $\mathcal{G}$ is the generalized Gaussian probability density function (GGPDF) defined as follows:

$$\mathcal{G}(x, \mu, \alpha, \beta) = \frac{\beta}{2\alpha\Gamma(\frac{1}{\beta})} e^{-(\frac{|x-\mu|}{\alpha})^\beta}$$

where $x, \mu, \alpha, \beta \in \mathbb{R}$ with $\alpha, \beta \geq 0$ and $\Gamma$ denotes the gamma function. This particular distribution includes the normal Gaussian distribution $\mathcal{N}$ when $\beta = 2$ (with mean $\mu$ and variance $\frac{\alpha^2}{2}$) and it includes also the Laplace distribution when $\beta = 1$.

Since the values of $r(t)$ and $\rho(t)$ given by the function $S$ are such that $0 \leq r \leq 1$ the range of values is rescaled in order to match the interval $[0, \psi]$ for $r$ and $[0, \xi]$ for $\rho$.

Using the parametric function $S$, we can generate several longitudinal lesions in different cross sections of a given fiber bundle. Since the longitudinal behavior of a lesion is not *a priori* predictable, the $\mu_r, \alpha_r, \beta_r$ and $\mu_\rho, \alpha_\rho, \beta_\rho$ parameters are randomly selected in order to simulate different kinds of longitudinal variations. Several examples of longitudinal simulated lesions are visible in Fig. 4.

The function $S$ could also be generalized in order to simulate appearing and disappearing lesions. The model could be easily extended by using a mixture of GGPDFs. The function $\mathcal{G}$ could then be replaced with $\mathcal{M}$ defined as

$$\mathcal{M}(x, \bar{\mu}, \bar{\alpha}, \bar{\beta}) = \sum_{i=1}^{v} \iota_i \frac{\beta_i}{2\alpha_i\Gamma(\frac{1}{\beta_i})} e^{-(\frac{|x-\mu_i|}{\alpha_i})^{\beta_i}}$$

where $v$ is the number of reappearing peaks of the lesions and $\iota_i \in \mathbb{R} | \sum_{i=1}^{v} \iota_i = 1$ is a weighting factor given to each mixture component.

The method could also be extended with other lesion shapes. For instance, an ellipsoid could be used to model the shape of the variation. In this case, the function $S$ could be extended to $S_{\text{ellipsoid}}$. This new function uses three different radii $r_1, r_2, r_3$, respectively, representing the size of the three axes of the ellipsoid.

In the rest of this paper, when we refer to the function $S$, we assume as GGPDF the function $\mathcal{G}$ and as lesion shape a sphere of radius $r$.

## III. Experiments

### A. Experiments on Simulated Longitudinal Variations

100 different longitudinal variations were simulated on the control subject's diffusion maps obtained using the model

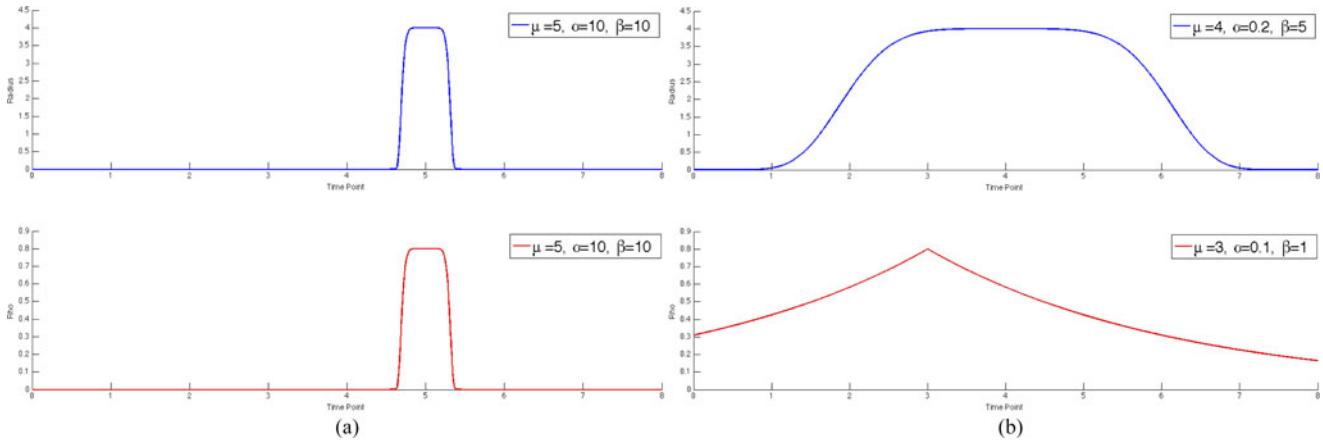



Fig. 4. Example of function $S$ corresponding to longitudinal simulated variations evolving in shape (blue function) and in reduction coefficient (red function). (a) Single time point appearing variation. (b) Variation with longitudinal stable shape (radius $r$) and evolving diffusion changes $\rho$.

described in Section II-F. All the variations were generated along ten different fiber bundles, namely, left and right, corticospinal tract, inferior-fronto occipital fasciculi, cingulum, and forceps major and minor of corpus callosum. In order to simulate small variations, we fixed $\psi = 2$ and $\xi = 0.5$. Since different NMF implementations performed differently according to the domain of application, as reported in [21] and [23], in this study, three different algorithms to compute NMF are used and compared: Alternating least-squares algorithm [24] (ALS), hierarchical alternating least-squares algorithm (HALS) [25], and multiplicative update (MUL) [18]. For each NMF analysis, the source and the abundance matrices were initialized randomly, the NMF procedure was repeated 20 times and the output with the best objective function value was withheld.

The capability to detect the presence of longitudinal variations was tested. For each algorithm, three different tests were performed: 1) binary classification for longitudinal detection, 2) find the time points affected by the longitudinal alterations, and 3) delineate the regions affected by the longitudinal changes. Each test was performed with $l = 1$ and $l = 2$ only. Due to the number of voxels in each cross section, with $l > 2$, we do not obtain enough voxels to apply NMF.

In order to find the best values of the threshold $\omega$, *MinPts* and the LOF different tests were performed using a range of values. The $\omega$-interval $(0.5 \leq \omega \leq 1)$ was divided into 11 steps, as a finer step size did not significantly improve the results any further. *MinPts* values range from 1 to 8 (the total number of time-points) and the LOF interval was given by $\{2, 2.5, 2.8, 3, 3.5, 3.8, 4, 4.5, 4.8\}$.

*1) Binary Classification for Longitudinal Detection:* In order to quantify how many simulated longitudinal variations were correctly identified by our method, we tested the capability of our method to detect if in a given cross-sectional longitudinal changes are present during the follow up. True positives (TP) and false negatives (FN) were computed to assess the Recall $(\frac{\mathrm{TP}}{\mathrm{TP+FN}})$.

*2) Longitudinal Change Detection:* We tested the capacity of our method to detect the time points affected by the longitudinal variations. More in detail, we check for each simulated variation, whether each time point is correctly classified as "normal" or "outlier." TP, false positives (FP), and FN were then used to compute the *F-Measure* $(\frac{2*\mathrm{TP}}{2*\mathrm{TP+FP+FN}})$ for the variation. Since multiple longitudinal variations were simulated along the fiber bundles, mean $(\overline{F-\mathrm{Measure}})$ and standard deviation $(\sigma(F-\mathrm{Measure}))$ of *F-Measure* were computed.

*3) Longitudinal Change Delineation:* We tested the capability of our method to well delineate the region affected by the longitudinal changes. In other words, we tested the capability of our algorithm to detect the simulated spherical regions in which we simulated the signal changes. In order to quantify the quality of the delineation, the Sørensen-dice score coefficient (DSC) [26] was computed according to the following equation:

$$\mathrm{DSC} = \frac{2 * |A \cap B|}{|A| + |B|}$$

where $A$ is the voxel set containing the regions with the simulated longitudinal variation and $B$ is the voxel set with the region detected by our method. According to this index, we can have following three different cases.

1) $\mathrm{DSC} = 0$: No overlap.
2) $0 < \mathrm{DSC} < 1$: Partial overlap.
3) $\mathrm{DSC} = 1$: Complete overlap.

Since multiple longitudinal variations were simulated along the fiber bundles, mean $(\overline{\mathrm{DSC}})$ and standard deviation $(\sigma(\mathrm{DSC}))$ of the DSC were computed.

In order to generalize the capability of the proposed method to detect longitudinal changes, two steps are performed. In the first step, a nested search of the parameters of the algorithm is performed, on simulated variations, for each combination of features and for each NMF algorithm. In the second step, the method was applied on a new set of simulated variations using the best parameters discovered in the first step.

## B. Experiments on Real MS Follow-up Data

Two RR MS patients (see Section II-D) were selected due to the presence of visible longitudinal alterations assessed by our neuroradiologist (FC). DTI data of each patient were processed

TABLE I
BEST VALUES OF RECALL, MEAN ($\overline{F-\text{MEASURE}}$, $\overline{\text{DSC}}$) AND STANDARD DEVIATION ($\sigma(F-\text{MEASURE})$, $\sigma(\text{DSC})$) IN PARENTHESIS OF *F-Measure* AND DSC FOR LONGITUDINAL TIME-POINTS IDENTIFICATION USING ONE LEVEL ($l=1$) AND DIFFERENT COMBINATIONS OF DIFFUSION PARAMETERS

| | | Recall | $\overline{F-\text{Measure}}$ | $\overline{\text{DSC}}$ |
|---|---|---|---|---|
| HALS | All | 0.68 | 0.72 (0.34) | 0.50 (0.27) |
| | KLA | 0.97 | 0.65 (0.25) | 0.25 (0.10) |
| | KLA, FA | 0.71 | 0.72 (0.32) | 0.29 (0.10) |
| | KLA, AA | 0.70 | 0.56 (0.20) | 0.24 (0.12) |
| | FA, MD, $\lambda_r$, $\lambda_2$, $\lambda_3$ | 0.67 | 0.56 (0.35) | 0.39 (0.25) |
| | FA | 0.88 | 0.74 (0.32) | 0.17 (0.26) |
| | MD | 0.71 | 0.52 (0.32) | 0.63 (0.34) |
| | FA, MD | 0.64 | 0.52 (0.37) | 0.31 (0.25) |
| | FA, MD, $\lambda_r$ | 0.70 | 0.54 (0.36) | 0.37 (0.24) |
| | $\lambda_2$, $\lambda_3$ | 0.72 | 0.66 (0.37) | 0.67 (0.30) |
| ALS | All | 0.71 | 0.52 (0.20) | 0.34 (0.15) |
| | KLA | 0.93 | 0.71 (0.20) | 0.26 (0.11) |
| | KLA, FA | 0.85 | 0.60 (0.18) | 0.30 (0.16) |
| | KLA, AA | 0.80 | 0.59 (0.20) | 0.35 (0.15) |
| | FA, MD, $\lambda_r$, $\lambda_2$, $\lambda_3$ | 0.70 | 0.57 (0.36) | 0.38 (0.25) |
| | FA | 0.80 | 0.78 (0.30) | 0.25 (0.32) |
| | MD | 0.72 | 0.64 (0.32) | 0.52 (0.35) |
| | FA, MD | 0.65 | 0.52 (0.35) | 0.35 (0.20) |
| | FA, MD, $\lambda_r$ | 0.68 | 0.53 (0.35) | 0.38 (0.24) |
| | $\lambda_2$, $\lambda_3$ | 0.82 | 0.70 (0.36) | 0.60 (0.33) |
| MUL | All | 0.62 | 0.54 (0.25) | 0.34 (0.15) |
| | KLA | 0.87 | 0.61 (0.22) | 0.32 (0.18) |
| | KLA, FA | 0.77 | 0.53 (0.20) | 0.30 (0.15) |
| | KLA, AA | 0.79 | 0.57 (0.24) | 0.23 (0.12) |
| | FA, MD, $\lambda_r$, $\lambda_2$, $\lambda_3$ | 0.69 | 0.54 (0.35) | 0.41 (0.28) |
| | FA | 0.86 | 0.68 (0.34) | 0.23 (0.32) |
| | MD | 0.74 | 0.62 (0.33) | 0.55 (0.31) |
| | FA, MD | 0.63 | 0.48 (0.38) | 0.33 (0.22) |
| | FA, MD, $\lambda_r$ | 0.67 | 0.55 (0.35) | 0.37 (0.22) |
| | $\lambda_2$, $\lambda_3$ | 0.71 | 0.74 (0.33) | 0.61 (0.33) |

TABLE II
BEST VALUES OF RECALL, MEAN ($\overline{F-\text{MEASURE}}$, $\overline{\text{DSC}}$) AND STANDARD DEVIATION ($\sigma(F-\text{MEASURE})$, $\sigma(\text{DSC})$) IN PARENTHESIS OF *F-Measure* AND DSC FOR LONGITUDINAL TIME-POINTS IDENTIFICATION USING TWO LEVELS ($l=2$) AND DIFFERENT COMBINATION OF DIFFUSION PARAMETERS

| | | Recall | $\overline{F-\text{Measure}}$ | $\overline{\text{DSC}}$ |
|---|---|---|---|---|
| HALS | All | 0.72 | 0.69 (0.25) | 0.52 (0.24) |
| | KLA | 0.99 | 0.48 (0.20) | 0.25 (0.12) |
| | KLA, FA | 0.99 | 0.50 (0.22) | 0.25 (0.11) |
| | KLA, AA | 0.99 | 0.52 (0.21) | 0.22 (0.09) |
| | FA, MD, $\lambda_r$, $\lambda_2$, $\lambda_3$ | 0.79 | 0.66 (0.34) | 0.54 (0.29) |
| | FA | 0.89 | 0.60 (0.33) | 0.21 (0.26) |
| | MD | 0.82 | 0.54 (0.31) | 0.40 (0.29) |
| | FA, MD | 0.72 | 0.68 (0.33) | 0.23 (0.23) |
| | FA, MD, $\lambda_r$ | 0.72 | 0.67 (0.35) | 0.46 (0.27) |
| | $\lambda_2$, $\lambda_3$ | 0.73 | 0.70 (0.26) | 0.57 (0.26) |
| ALS | All | 0.75 | 0.62 (0.22) | 0.36 (0.10) |
| | KLA | 0.94 | 0.55 (0.23) | 0.30 (0.12) |
| | KLA, FA | 0.99 | 0.49 (0.20) | 0.30 (0.19) |
| | KLA, AA | 0.97 | 0.52 (0.21) | 0.29 (0.15) |
| | FA, MD, $\lambda_r$, $\lambda_2$, $\lambda_3$ | 0.75 | 0.68 (0.32) | 0.48 (0.30) |
| | FA | 0.88 | 0.63 (0.32) | 0.18 (0.24) |
| | MD | 0.86 | 0.56 (0.35) | 0.47 (0.31) |
| | FA, MD | 0.74 | 0.66 (0.33) | 0.34 (0.28) |
| | FA, MD, $\lambda_r$ | 0.72 | 0.67 (0.34) | 0.39 (0.34) |
| | $\lambda_2$, $\lambda_3$ | 0.80 | 0.68 (0.33) | 0.59 (0.29) |
| MUL | All | 0.86 | 0.64 (0.21) | 0.40 (0.20) |
| | KLA | 0.98 | 0.48 (0.22) | 0.26 (0.12) |
| | KLA, FA | 0.98 | 0.51 (0.25) | 0.27 (0.15) |
| | KLA, AA | 0.94 | 0.42 (0.21) | 0.26 (0.11) |
| | FA, MD, $\lambda_r$, $\lambda_2$, $\lambda_3$ | 0.75 | 0.66 (0.33) | 0.51 (0.27) |
| | FA | 0.97 | 0.52 (0.25) | 0.29 (0.25) |
| | MD | 0.82 | 0.53 (0.32) | 0.43 (0.28) |
| | FA, MD | 0.73 | 0.60 (0.35) | 0.34 (0.27) |
| | FA, MD, $\lambda_r$ | 0.71 | 0.69 (0.32) | 0.42 (0.30) |
| | $\lambda_2$, $\lambda_3$ | 0.75 | 0.74 (0.30) | 0.61 (0.25) |

using our proposed pipeline described in Section II. Among the 20 fiber bundles (contained in the JHU atlas), the cortico-spinal tract (CST) was selected by our neuroradiologist (FC) because of the presence of longitudinal MS alterations.

## IV. RESULTS

### A. Results on Simulated Longitudinal Variations

Best results for all three experiments, described previously in Section III, are reported in Table I for $l=1$ and in Table II for $l=2$. In these tables, we show how, for each combination of diffusion parameters and for each NMF algorithm, different performances were obtained. In the tables, we denote with "All" the case obtained when all seven diffusion parameters (FA, MD, $\lambda_2$, $\lambda_3$, $\lambda_r$, KLA, AAA) are used as features.

For $l=1$, best results in terms of Recall are obtained using the HALS algorithm with the KLA as feature (0.97). Best $\overline{\text{DSC}}$ (0.67) is obtained using the HALS algorithm and $\lambda_2$, $\lambda_3$ as features, while best $\overline{F-\text{Measure}}$ (0.78) is obtained using the ALS algorithm and FA as feature. Compared to the other algorithms and features, ALS globally shows a better capability to delineate the longitudinal evolutions with high values of Recall (0.82), $\overline{F-\text{Measure}}$ (0.70) and $\overline{\text{DSC}}$ (0.60) reached using $\lambda_2, \lambda_3$ as features and with the following parameters: $\omega=0.55$, MinPts $=3$, and LOF $=2.5$. With respect to the other two algorithms, MUL shows comparable performances.

For $l=2$, similar results are obtained for HALS, ALS, and MUL having, respectively, 0.73, 0.80, and 0.75 as Recall, 0.70, 0.68, and 0.74 as $\overline{F-\text{Measure}}$, and 0.57, 0.59, and 0.61 as $\overline{\text{DSC}}$ with $\lambda_2$ and $\lambda_3$ as features. Moreover, as for $l=1$, the HALS algorithm shows the highest performances in terms of Recall (0.99) with the following three features' sets 1) KLA 2) KLA, FA, and 3) KLA, AA. Also the ALS algorithm reaches a high value of Recall (0.99) but just having as feature KLA, FA.

In Tables III–V, we show how the time-point detection and delineation performances change according to $\omega$, *LOF*, and *MinPts* parameters.

We tested our method with different parameters by using the MUL algorithm and two levels ($l=2$) with a feature vector composed of FA, MD, $\lambda_r$, $\lambda_2$, and $\lambda_3$. Values with $7 \leq$ MinPts $\leq 8$ are not shown in the tables since for these parameters the values are all zero. As expected, the $\omega$ parameter mainly influences the $\overline{\text{DSC}}$ performances. Low values of $\omega$ ($0.5 \leq \omega \leq 0.6$) show high $\overline{\text{DSC}}$ values, while, large values of $\omega$ ($\omega \geq 0.65$) yield a degradation of the $\overline{\text{DSC}}$ performances. This behavior is justified by the fact that the $\omega$ parameter is used as threshold to decide which voxels should be selected from the abundance vectors.

In addition, *LOF* and *MinPts* parameters are used for the LOF outlier detection algorithm, and they mainly influence the

TABLE III
RECALL FOR AFFECTED TIME-POINTS IDENTIFICATION USING MUL ALGORITHM WITH TWO LEVELS ($l=2$) AND USING FA, MD, $\lambda_r, \lambda_2, \lambda_3$ ($m=5$) AS FEATURES

| | Recall | | | | | | | | | | | | | | | | | | | | | | | | | | | |
|---|---|---|---|---|---|---|---|---|---|---|---|---|---|---|---|---|---|---|---|---|---|---|---|---|---|---|---|---|
| | $\omega \geq 0.50$ | | | | | | $\omega \geq 0.55$ | | | | | | $\omega \geq 0.60$ | | | | | | $\omega \geq 0.65$ | | | | | | $\omega \geq 0.70$ | | | | | |
| LOF \ MinPts | 1 | 2 | 3 | 4 | 5 | 6 | 1 | 2 | 3 | 4 | 5 | 6 | 1 | 2 | 3 | 4 | 5 | 6 | 1 | 2 | 3 | 4 | 5 | 6 | 1 | 2 | 3 | 4 | 5 | 6 |
| **2** | 0.97 | 0.97 | 0.94 | 0.86 | 0.63 | 0.42 | 0.95 | 0.95 | 0.94 | 0.91 | 0.68 | 0.38 | 0.94 | 0.94 | 0.88 | 0.81 | 0.52 | 0.29 | 0.90 | 0.90 | 0.85 | 0.79 | 0.54 | 0.19 | 0.86 | 0.86 | 0.81 | 0.70 | 0.44 | 0.23 |
| **2.5** | 0.86 | 0.86 | 0.83 | 0.78 | 0.51 | 0.32 | 0.88 | 0.88 | 0.86 | 0.81 | 0.51 | 0.26 | 0.86 | 0.86 | 0.79 | 0.73 | 0.39 | 0.22 | 0.83 | 0.83 | 0.77 | 0.65 | 0.36 | 0.15 | 0.77 | 0.77 | 0.73 | 0.64 | 0.35 | 0.15 |
| **2.8** | 0.82 | 0.82 | 0.78 | 0.75 | 0.48 | 0.29 | 0.85 | 0.85 | 0.81 | 0.76 | 0.45 | 0.22 | 0.82 | 0.82 | 0.75 | 0.69 | 0.35 | 0.18 | 0.80 | 0.80 | 0.74 | 0.63 | 0.30 | 0.14 | 0.73 | 0.73 | 0.69 | 0.62 | 0.29 | 0.13 |
| **3** | 0.78 | 0.78 | 0.76 | 0.72 | 0.45 | 0.26 | 0.84 | 0.84 | 0.79 | 0.75 | 0.41 | 0.19 | 0.78 | 0.78 | 0.72 | 0.66 | 0.35 | 0.18 | 0.75 | 0.75 | 0.69 | 0.60 | 0.25 | 0.13 | 0.71 | 0.71 | 0.67 | 0.60 | 0.27 | 0.12 |
| **3.5** | 0.75 | 0.75 | 0.73 | 0.68 | 0.41 | 0.20 | 0.78 | 0.78 | 0.73 | 0.68 | 0.35 | 0.16 | 0.70 | 0.70 | 0.67 | 0.61 | 0.29 | 0.13 | 0.63 | 0.63 | 0.60 | 0.55 | 0.21 | 0.11 | 0.65 | 0.65 | 0.61 | 0.53 | 0.22 | 0.10 |
| **3.8** | 0.70 | 0.70 | 0.68 | 0.64 | 0.39 | 0.20 | 0.75 | 0.75 | 0.71 | 0.64 | 0.30 | 0.16 | 0.68 | 0.68 | 0.62 | 0.56 | 0.27 | 0.09 | 0.59 | 0.59 | 0.57 | 0.51 | 0.18 | 0.11 | 0.58 | 0.58 | 0.57 | 0.47 | 0.18 | 0.09 |
| **4** | 0.70 | 0.70 | 0.68 | 0.64 | 0.38 | 0.17 | 0.71 | 0.71 | 0.67 | 0.60 | 0.30 | 0.16 | 0.66 | 0.66 | 0.62 | 0.56 | 0.24 | 0.09 | 0.55 | 0.55 | 0.54 | 0.46 | 0.17 | 0.10 | 0.54 | 0.54 | 0.53 | 0.43 | 0.17 | 0.08 |
| **4.5** | 0.64 | 0.64 | 0.60 | 0.57 | 0.32 | 0.15 | 0.69 | 0.69 | 0.65 | 0.54 | 0.26 | 0.14 | 0.58 | 0.58 | 0.56 | 0.48 | 0.22 | 0.08 | 0.47 | 0.47 | 0.46 | 0.41 | 0.15 | 0.10 | 0.51 | 0.51 | 0.48 | 0.42 | 0.14 | 0.08 |
| **4.8** | 0.61 | 0.61 | 0.56 | 0.51 | 0.27 | 0.13 | 0.66 | 0.66 | 0.64 | 0.53 | 0.24 | 0.13 | 0.56 | 0.56 | 0.55 | 0.47 | 0.17 | 0.08 | 0.47 | 0.47 | 0.46 | 0.40 | 0.14 | 0.08 | 0.51 | 0.51 | 0.48 | 0.39 | 0.12 | 0.08 |

TABLE IV
CHANGES IN MEAN F-MEASURE ($\overline{F-\text{MEASURE}}$) FOR AFFECTED TIME-POINTS IDENTIFICATION USING MUL ALGORITHM WITH TWO LEVELS ($l=2$) AND USING FA, MD, $\lambda_r, \lambda_2, \lambda_3$ ($m=5$) AS FEATURES

| | $\overline{F-Measure}$ | | | | | | | | | | | | | | | | | | | | | | | | | | | |
|---|---|---|---|---|---|---|---|---|---|---|---|---|---|---|---|---|---|---|---|---|---|---|---|---|---|---|---|---|
| | $\omega \geq 0.50$ | | | | | | $\omega \geq 0.55$ | | | | | | $\omega \geq 0.60$ | | | | | | $\omega \geq 0.65$ | | | | | | $\omega \geq 0.70$ | | | | | |
| LOF \ MinPts | 1 | 2 | 3 | 4 | 5 | 6 | 1 | 2 | 3 | 4 | 5 | 6 | 1 | 2 | 3 | 4 | 5 | 6 | 1 | 2 | 3 | 4 | 5 | 6 | 1 | 2 | 3 | 4 | 5 | 6 |
| **2** | 0.58 | 0.58 | 0.60 | 0.65 | 0.59 | 0.60 | 0.55 | 0.55 | 0.59 | 0.62 | 0.58 | 0.60 | 0.55 | 0.55 | 0.60 | 0.66 | 0.62 | 0.63 | 0.54 | 0.54 | 0.60 | 0.64 | 0.59 | 0.78 | 0.57 | 0.57 | 0.62 | 0.72 | 0.64 | 0.57 |
| **2.5** | 0.64 | 0.64 | 0.67 | 0.73 | 0.66 | 0.59 | 0.58 | 0.58 | 0.61 | 0.67 | 0.60 | 0.60 | 0.63 | 0.63 | 0.69 | 0.72 | 0.66 | 0.67 | 0.58 | 0.58 | 0.66 | 0.75 | 0.65 | 0.78 | 0.61 | 0.61 | 0.66 | 0.72 | 0.62 | 0.63 |
| **2.8** | 0.65 | 0.65 | 0.70 | 0.74 | 0.65 | 0.62 | 0.60 | 0.60 | 0.64 | 0.70 | 0.64 | 0.63 | 0.65 | 0.65 | 0.71 | 0.73 | 0.68 | 0.71 | 0.61 | 0.61 | 0.69 | 0.74 | 0.71 | 0.76 | 0.62 | 0.62 | 0.69 | 0.71 | 0.66 | 0.69 |
| **3** | 0.68 | 0.68 | 0.72 | 0.74 | 0.66 | 0.62 | 0.61 | 0.61 | 0.65 | 0.70 | 0.67 | 0.65 | 0.66 | 0.66 | 0.71 | 0.76 | 0.68 | 0.71 | 0.61 | 0.61 | 0.70 | 0.76 | 0.68 | 0.78 | 0.63 | 0.63 | 0.69 | 0.73 | 0.68 | 0.71 |
| **3.5** | 0.68 | 0.68 | 0.72 | 0.73 | 0.68 | 0.67 | 0.63 | 0.63 | 0.67 | 0.70 | 0.67 | 0.69 | 0.69 | 0.68 | 0.71 | 0.75 | 0.71 | 0.71 | 0.66 | 0.66 | 0.73 | 0.75 | 0.70 | 0.74 | 0.66 | 0.66 | 0.72 | 0.76 | 0.72 | 0.70 |
| **3.8** | 0.68 | 0.68 | 0.71 | 0.73 | 0.66 | 0.67 | 0.64 | 0.64 | 0.68 | 0.73 | 0.70 | 0.69 | 0.69 | 0.69 | 0.74 | 0.75 | 0.73 | 0.72 | 0.66 | 0.66 | 0.70 | 0.73 | 0.74 | 0.74 | 0.69 | 0.69 | 0.72 | 0.78 | 0.72 | 0.72 |
| **4** | 0.68 | 0.68 | 0.71 | 0.72 | 0.65 | 0.68 | 0.66 | 0.66 | 0.70 | 0.74 | 0.74 | 0.73 | 0.69 | 0.69 | 0.72 | 0.74 | 0.78 | 0.72 | 0.70 | 0.70 | 0.73 | 0.78 | 0.75 | 0.72 | 0.69 | 0.69 | 0.72 | 0.77 | 0.74 | 0.75 |
| **4.5** | 0.66 | 0.66 | 0.71 | 0.73 | 0.70 | 0.69 | 0.66 | 0.66 | 0.68 | 0.74 | 0.71 | 0.73 | 0.74 | 0.74 | 0.75 | 0.80 | 0.79 | 0.75 | 0.73 | 0.73 | 0.76 | 0.77 | 0.77 | 0.72 | 0.69 | 0.69 | 0.74 | 0.76 | 0.79 | 0.75 |
| **4.8** | 0.66 | 0.66 | 0.71 | 0.73 | 0.70 | 0.68 | 0.66 | 0.66 | 0.67 | 0.75 | 0.69 | 0.73 | 0.73 | 0.73 | 0.74 | 0.81 | 0.84 | 0.75 | 0.73 | 0.73 | 0.75 | 0.76 | 0.77 | 0.75 | 0.68 | 0.68 | 0.74 | 0.76 | 0.79 | 0.75 |

TABLE V
CHANGES IN MEAN DSC ($\overline{\text{DSC}}$) FOR AFFECTED TIME-POINTS DELINEATION USING MUL ALGORITHM WITH TWO LEVELS ($l=2$) AND USING FA, MD, $\lambda_r, \lambda_2, \lambda_3$ ($m=5$) AS FEATURES

| | $\overline{DSC}$ | | | | | | | | | | | | | | | | | | | | | | | | | | | |
|---|---|---|---|---|---|---|---|---|---|---|---|---|---|---|---|---|---|---|---|---|---|---|---|---|---|---|---|---|
| | $\omega \geq 0.50$ | | | | | | $\omega \geq 0.55$ | | | | | | $\omega \geq 0.60$ | | | | | | $\omega \geq 0.65$ | | | | | | $\omega \geq 0.70$ | | | | | |
| LOF \ MinPts | 1 | 2 | 3 | 4 | 5 | 6 | 1 | 2 | 3 | 4 | 5 | 6 | 1 | 2 | 3 | 4 | 5 | 6 | 1 | 2 | 3 | 4 | 5 | 6 | 1 | 2 | 3 | 4 | 5 | 6 |
| **2** | 0.49 | 0.49 | 0.51 | 0.56 | 0.51 | 0.54 | 0.40 | 0.40 | 0.43 | 0.46 | 0.46 | 0.49 | 0.34 | 0.34 | 0.37 | 0.40 | 0.43 | 0.45 | 0.25 | 0.25 | 0.27 | 0.28 | 0.26 | 0.38 | 0.14 | 0.14 | 0.14 | 0.17 | 0.19 | 0.21 |
| **2.5** | 0.54 | 0.54 | 0.56 | 0.61 | 0.56 | 0.59 | 0.43 | 0.43 | 0.46 | 0.51 | 0.48 | 0.51 | 0.38 | 0.39 | 0.41 | 0.43 | 0.44 | 0.50 | 0.26 | 0.26 | 0.28 | 0.31 | 0.30 | 0.33 | 0.15 | 0.15 | 0.15 | 0.17 | 0.19 | 0.20 |
| **2.8** | 0.55 | 0.55 | 0.58 | 0.61 | 0.55 | 0.59 | 0.45 | 0.45 | 0.48 | 0.54 | 0.51 | 0.51 | 0.39 | 0.39 | 0.43 | 0.45 | 0.45 | 0.51 | 0.27 | 0.27 | 0.29 | 0.31 | 0.27 | 0.34 | 0.14 | 0.14 | 0.16 | 0.17 | 0.20 | 0.21 |
| **3** | 0.57 | 0.57 | 0.58 | 0.61 | 0.55 | 0.58 | 0.44 | 0.44 | 0.48 | 0.53 | 0.53 | 0.55 | 0.41 | 0.41 | 0.44 | 0.46 | 0.45 | 0.51 | 0.27 | 0.27 | 0.29 | 0.31 | 0.28 | 0.34 | 0.14 | 0.14 | 0.16 | 0.18 | 0.22 | 0.23 |
| **3.5** | 0.57 | 0.57 | 0.60 | 0.62 | 0.60 | 0.66 | 0.46 | 0.46 | 0.50 | 0.53 | 0.55 | 0.58 | 0.41 | 0.41 | 0.43 | 0.45 | 0.50 | 0.49 | 0.30 | 0.30 | 0.31 | 0.31 | 0.32 | 0.37 | 0.16 | 0.16 | 0.17 | 0.18 | 0.23 | 0.22 |
| **3.8** | 0.60 | 0.60 | 0.62 | 0.61 | 0.60 | 0.66 | 0.47 | 0.47 | 0.51 | 0.56 | 0.53 | 0.58 | 0.40 | 0.40 | 0.44 | 0.45 | 0.51 | 0.53 | 0.31 | 0.31 | 0.32 | 0.32 | 0.35 | 0.37 | 0.18 | 0.18 | 0.18 | 0.20 | 0.24 | 0.24 |
| **4** | 0.60 | 0.60 | 0.62 | 0.61 | 0.60 | 0.70 | 0.49 | 0.49 | 0.54 | 0.57 | 0.55 | 0.58 | 0.42 | 0.42 | 0.44 | 0.45 | 0.53 | 0.53 | 0.32 | 0.32 | 0.33 | 0.34 | 0.36 | 0.36 | 0.18 | 0.18 | 0.19 | 0.20 | 0.25 | 0.25 |
| **4.5** | 0.58 | 0.58 | 0.61 | 0.60 | 0.60 | 0.72 | 0.48 | 0.48 | 0.52 | 0.56 | 0.60 | 0.60 | 0.45 | 0.45 | 0.46 | 0.48 | 0.54 | 0.56 | 0.32 | 0.32 | 0.33 | 0.34 | 0.37 | 0.36 | 0.18 | 0.18 | 0.20 | 0.20 | 0.27 | 0.25 |
| **4.8** | 0.58 | 0.57 | 0.61 | 0.61 | 0.62 | 0.73 | 0.50 | 0.50 | 0.52 | 0.57 | 0.60 | 0.61 | 0.45 | 0.45 | 0.46 | 0.48 | 0.60 | 0.56 | 0.33 | 0.33 | 0.33 | 0.34 | 0.39 | 0.43 | 0.18 | 0.18 | 0.20 | 0.20 | 0.32 | 0.25 |

Recall and $\overline{F-\text{Measure}}$ performances. With $1 \leq \text{MinPts} \leq 4$ and $2 \leq \text{LOF} \leq 3.8$ high values of Recall and $\overline{F-\text{Measure}}$ are obtained.

### B. Results on Real MS Follow-up Data

In order to show how the combination of the five diffusion parameters could be helpful in application on real data, a feature vector composed by FA, MD, $\lambda_r$, $\lambda_2$, and $\lambda_3$ ($m=5$) was used. Based on the results obtained in the simulated validation, we used HALS as algorithm since it globally reached, for these five features, the best results in the three tests. The following parameters $l=2, \text{LOF}=2.8,$ and $\text{MinPts}=4$ were selected.

As illustrated in Figs. 5 and 6, both small and large "pathological" longitudinal variations occurring along the two WM fiber bundles were correctly identified using the proposed method. In both figures, it is possible to see how MS modifies, longitudinally, the diffusion values in a specific WM region. With our method, it is possible to identify where these regions are located along specific WM fiber bundles and which part of these bundles are affected by the longitudinal changes. We can thus extract two types of information: 1) segmentation of the regions affected by the longitudinal variations and 2) the delineation of the time points affected by the longitudinal variations. Detection of significant changes were validated by our neuroradiologist (FC).

## V. DISCUSSION

We described a new fully automated tool to analyze longitudinal changes in the WM fiber bundles of MS patients. Particularly, we developed a new NMF-based method to detect local scale longitudinal variations caused by rapid inflammatory processes in MS patients. The fully automated method described in this paper is divided in three major steps: 1) preprocessing of longitudinal diffusion acquisitions, 2) WM fiber bundles extraction, and 3) application of NMF and LOF cluster algorithm to detect and delineate longitudinal variations appearing in the cross section of the given WM fiber bundle. Moreover, in order to test the capability of our method to detect and delineate longitudinal changes, a new simulation paradigm is introduced. The new simulation method LVS allows to replicate real longitudinal variations occurring in diffusion data in MS patients. The method uses the longitudinal data of a control subject to simulate longitudinal variations in shape and signal by following a GGPDF distribution.

Results on simulated data show the capability of our method to detect and delineate the presence of longitudinal changes in cross sections of WM fiber bundles. The experiment section was also enriched by the analysis of the features set and the input parameters of our method. This process allowed us to see how the performance of our method changes according to the parameters, and which range of parameters gives the best results in

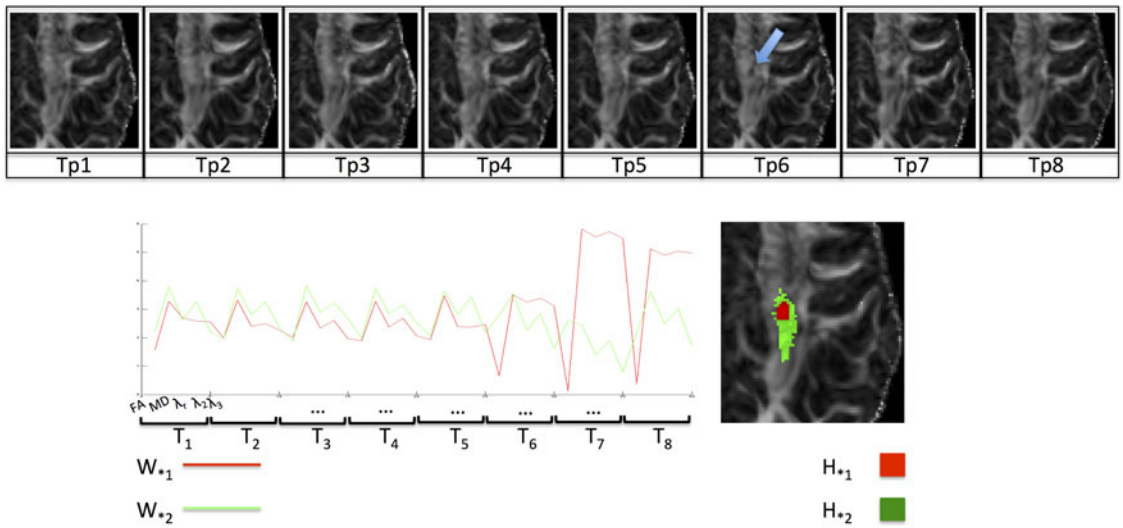



Fig. 5. Longitudinal variations detected (in red) by the application of our method on left CST of an MS patient. On top, the longitudinal evolution of the FA signal is visible. Starting from time point 6, a variation, given by the presence of a new MS lesion, is visible. On bottom, the application of our NMF-based method shows how in the source matrix irregularities are visible starting from time point 6 to time point 8. In parallel, the abundance matrix shows the delineation of the region affected by the longitudinal variation (red) and the regions not affected by the longitudinal variation (green).

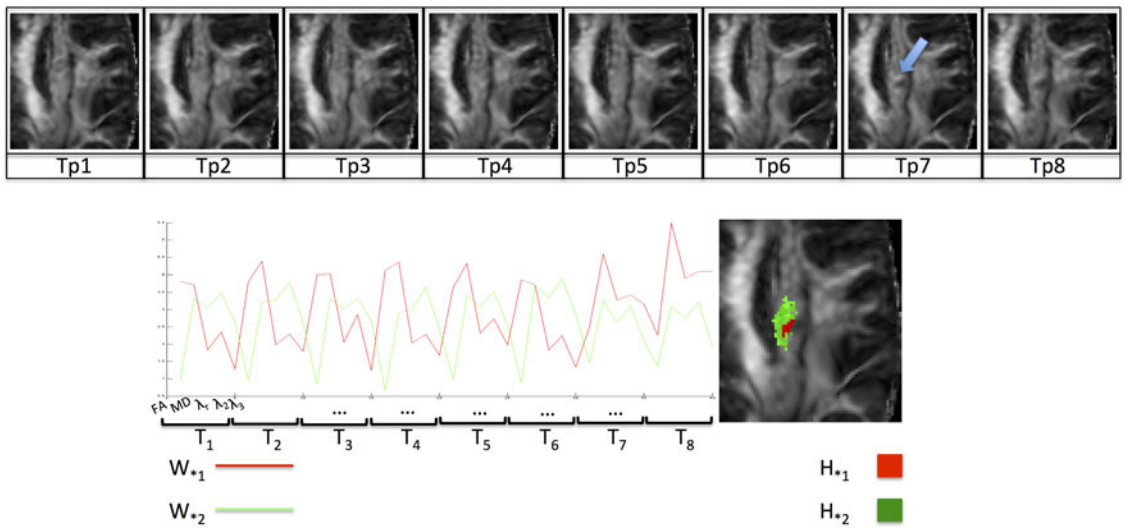



Fig. 6. Longitudinal variations detected (in red) by the application of our method on left CST of an MS patient. On top, the longitudinal evolution of the FA signal is visible. Starting from time point 7, a variation, given by the presence of a new MS lesion, is visible. On bottom, the application of our NMF-based method shows how in the source matrix irregularities are visible starting from time point 7 to time point 8. In parallel, the abundance matrix shows the delineation of the region affected by the longitudinal variation (red) and the regions not affected by the longitudinal variation (green).

terms of detection and delineation. As a result of this validation step, we obtained that good improvements were reached using two levels ($l = 2$) compared to the one level analysis $l = 1$. Moreover this validation process gave us the possibility to explore how certain parameters like *LOF* and MinPts influence performances like Recall and $\overline{F-\text{Measure}}$.

Those parameters can also be adjusted in order to adapt the proposed method to different situations. For instance, for the analysis of thin fiber bundles, where the number of the voxels in the cross section is small, the number of levels in the tree can be set to one ($l = 1$).

The features used to perform the analysis play also an important role on the final results. It is possible to see how the introduction of KLA and AA allows to obtain excellent results in terms of $\overline{F-\text{Measure}}$ compared to the "standard" DTI derived metrics for $l = 1$ and $l = 2$. Globally the optimal results are reached using $\lambda_2$ and $\lambda_3$ as feature set. The introduction of other diffusion parameters does not drastically improves the performance. Moreover, from the results obtained on the simulated data, we can observe two principal characteristics. First, ALS is the best algorithm to detect if longitudinal changes are present in the follow-up. Second, MUL is the best to detect the time points affected by the changes and segment the affected voxels.

One limitation present in this study is related to the low value of $\overline{\text{DSC}}$ reached by our method. In future work, we plan to

overcome this limitation by using structural information derived from classical MRI sequences like T1, T2 FLAIR, etc.

As final experimental step, the proposed method was applied in real MS patients showing its capability to detect and delineate the temporal and spatial changes observed by the neuroradiologist.

Another interesting added value of our method is its capability to easily include new time points acquired later in time. Indeed, due to the robustness of the registration pipeline used in this study [11], the effects of certain longitudinal biases [8], like atrophy, are minimized.

Compared to the other methods already presented in the literature [7], [6], [9], the proposed method allows to overcome multiple limitations. First, it allows to analyze multiple DTI maps taking into account more than two time points. Second, it not only allows to delineate the regions affected by the longitudinal changes, but also to show which time points are affected by those changes. Third, the method is unsupervised. Hence, there is no need to formulate particular hypotheses about the distribution and/or evolution of the diffusion parameters. Finally, it could be easily extended to include other modalities without modifying the algorithm and without formulating new hypotheses about the modalities' signal distribution and/or evolution.

## VI. Conclusion

In this study, a new pipeline for longitudinal analysis of changes along WM fiber bundles was presented. We showed how NMF, in combination with LOF, is a powerful tool to discover the presence of longitudinal variations. The method was tested on simulated data, generated with a new simulation paradigm, and on real data.

Results suggested that the proposed method is a promising tool to longitudinal analysis of fiber bundles in neurodegenerative diseases like MS.

Encouraged by those preliminary results, as for future work, we plan to extend the application of our method to perform multimodal analysis. The idea is to apply the algorithm on different MRI modalities (MRS, T2, T1, etc.) and other diffusion metrics to quantify anisotropy [13] like Aitchison anisotropy, shape anisotropy and others in order to discover the optimal set of features to perform longitudinal analysis.

## Acknowledgment

This paper reflects only the authors' views and the Union is not liable for any use that may be made of the contained information.

## References

[1] M. Vandermosten *et al.*, "A DTI tractography study in pre-readers at risk for dyslexia," *Developmental Cogn. Neurosc.*, vol. 14, pp. 8–15, 2015.
[2] E. Mak, L. Su, G. B. Williams, and J. T. O'Brien, "Neuroimaging correlates of cognitive impairment and dementia in Parkinson's disease," *Parkinsonism Related Disorders*, vol. 21, no. 8, pp. 862–870, 2015.
[3] S. Mesaros *et al.*, "Thalamic damage predicts the evolution of primary-progressive multiple sclerosis at 5 years," *Amer. J. Neuroradiol.*, vol. 32, no. 6, pp. 1016–1020, 2011.
[4] A. Rovira, C. Auger, and J. Alonso, "Magnetic resonance monitoring of lesion evolution in multiple sclerosis," *Therapeutics Advances Neurol. Disorders*, vol. 6, no. 5, pp. 298–310, 2013.
[5] S. Mori, B. J. Crain, V. P. Chacko, and P. C. van Zijl, "Three-dimensional tracking of axonal projections in the brain by magnetic resonance imaging," *Ann. Neurol.*, vol. 45, pp. 265–269, 1999.
[6] C. Stamile *et al.*, "A sensitive and automatic white matter fiber tracts model for longitudinal analysis of diffusion tensor images in multiple sclerosis," *PLoS ONE*, vol. 11, no. 5, e0156405, 2016. doi:10.1371/journal.pone.0156405.
[7] A. Grigis *et al.*, "Longitudinal change detection: Inference on the diffusion tensor along white matter pathways," *Med. Image Anal.*, vol. 17, pp. 375–386, 2013.
[8] M. Reuter, N. J. Schmansky, H. D. Rosas, and B. Fischl, "Within-subject template estimation for unbiased longitudinal image analysis," *Neuroimage*, vol. 61, no. 4, pp. 1402–1418, 2012.
[9] C. Stamile *et al.*, "A longitudinal model for variations detection in white matter fiber-bundles," in *Proc. Int. Conf. Syst., Signals Image Process.*, 2015, pp. 57–60.
[10] M. Jenkinson and S. Smith, "A global optimisation method for robust affine registration of brain images," *Med. Image Anal.*, vol. 5, pp. 143–156, 2001.
[11] S. Keihaninejad *et al.*, "An unbiased longitudinal analysis framework for tracking white matter changes using diffusion tensor imaging with application to Alzheimer's disease," *Neuroimage*, vol. 72, pp. 153–163, 2013.
[12] A. Varentsova, S. Zhang, and K. Arfanakis, "Development of a high angular resolution diffusion imaging human brain template," *Neuroimage*, vol. 91, pp. 177–186, 2014.
[13] F. Prados *et al.*, "Analysis of new diffusion tensor imaging anisotropy measures in the three-phase plot," *J. Magn. Reson. Imag.*, vol. 31, pp. 1435–1444, 2010.
[14] J. D. Tournier, F. Calamante, and A. Connelly, "MRtrix: Diffusion tractography in crossing fiber regions," *Int. J. Imag. Syst. Technol.*, vol. 22, pp. 53–66, 2012.
[15] C. Stamile *et al.*, "A model-guided string-based approach to white matter fiber-bundles extraction," in *Brain Informatics and Health* (Lecture Notes in Computer Science). Switzerland: Springer, 2015, pp. 135–144.
[16] K. Hua *et al.* "Tract probability maps in stereotaxic spaces: Analyses of white matter anatomy and tract-specific quantification," *Neuroimage*, vol. 39, pp. 336–347, 2008.
[17] J. MacQueen, "Some methods for classification and analysis of multivariate observations," in *Proc. 5th Berkeley Symp. Math. Statist. Probab.*, vol. 1, no. 14, 1967, pp. 281–297.
[18] D. D. Lee and H. S. Seung, "Learning the parts of objects by non-negative matrix factorization," *Nature*, vol. 401, pp. 788–791, 1999.
[19] S. Ortega-Martorell *et al.*, "Convex non-negative matrix factorization for brain tumor delimitation from MRSI data," *PloS One*, vol. 7, no. 10, 2012.
[20] P. Sajda *et al.*, "Nonnegative matrix factorization for rapid recovery of constituent spectra in magnetic resonance chemical shift imaging of the brain," *IEEE Trans. Med. Imag.*, vol. 23, pp. 1453–1465, 2004.
[21] N. Sauwen *et al.*, "Hierarchical non-negative matrix factorization to characterize brain tumor heterogeneity using multi-parametric MRI," *NMR Biomed.*, vol. 28, no. 12, pp. 1599–1624, 2015.
[22] M. M. Breunig, H. -P. Kriegel, R. T. Ng, and J. Sander, "LOF: Identifying density-based local outliers," *ACM SIGMOD*, vol. 29, pp. 93–104, 2000.
[23] Y. Li, D. Sima, S. Van Cauter, U. Himmelreich, Y. Pi, and S. Van Huffel, "Simulation study of tissue type differentiation using non-negative matrix factorization," in *Proc. Int. Conf. Bio-Inspired Syst. Signal Process.*, 2012, pp. 212–217.
[24] N. Gillis and F. Glineur, "Accelerated multiplicative updates and hierarchical ALS algorithms for nonnegative matrix factorization," *Neural Comput.*, vol. 24, pp. 1085–1105, 2012.
[25] A. Cichocki and A. H. Phan, "Fast local algorithms for large scale nonnegative matrix and tensor factorizations," *IEICE Trans. Fundam. Electron.*, vol. 92, no. 3, pp. 708–721, 2009.
[26] K. H. Zou *et al.*, "Statistical validation of image segmentation quality based on a spatial overlap index," *Acad. Radiol.*, vol. 11, no. 2, pp. 178–189, 2004.

Authors' photographs and biographies are not available at the time of publication.